A FAST COVARIANCE MATRIX RECONSTRUCTION METHOD FOR TWO-DIMENSIONAL DIRECTION-OF-ARRIVAL ESTIMATION

Xiaohuan Wu[1], *Wei-Ping Zhu*[1,2] *and Jun Yan*[1]

[1]Key Lab of Broadband Wireless Communication and Sensor Network Technology,
Nanjing University of Posts and Telecommunications, Nanjing, China
[2]Department of Electrical and Computer Engineering,
Concordia University, Montreal, Canada
Email: {2013010101, zwp, yanj}@njupt.edu.cn

ABSTRACT

In this paper, a new method for two-dimensional (2-D) direction-of-arrival (DOA) estimation is proposed. We first reconstruct the covariance matrix of the coarray with block-Toeplitz structure and then retrieve the DOAs. Our method is computationally efficient as supported by the derived closed-form expression for the estimated covariance matrix. Unlike other methods, which require fully loaded arrays, the proposed method can be applied in the case of common rectangular arrays with arbitrary geometries. The estimated azimuth and elevation angles are automatically paired. Moreover, our method is of high estimation accuracy and immune to the angle ambiguity effect. Numerical simulations are carried out to verify the effectiveness of the proposed method.

Index Terms— 2-D DOA estimation, Toeplitz-block-Toeplitz structure, generalized rectangular array (GRA)

1. INTRODUCTION

The problem of two-dimensional (2-D) direction-of-arrival (DOA) estimation, where both azimuth and elevation angles of the incident signals are estimated jointly by using a planar array, has been attracted much attention in recent years. The selection of the array geometry largely affects the estimation accuracy and computational efficiency and thus has been extensively investigated in literature [1–3]. In particular, the uniform rectangular array (URA) can be regarded as the 2-D extension of the uniform linear array (ULA) and hence several computationally efficient methods have been proposed for 2-D DOA estimation in URAs [4], [1], among which the 2-D ESPRIT [4] is an easy-to-implement algorithm since the shift invariance property of the array output. However, the 2-D ESPRIT is not applicable to a sparse rectangular array (SRA) where the sensors are not fully implemented. The classic types of SRAs are L/T-shaped array and cross array [5], among which the L-shaped array has the best estimation performance owing to its larger array aperture as defined by the largest distance among the sensors [6]. In addition, many methods have been proposed by exploring the structured information of the array geometry. For instance, in the L-shaped array, since the cross-correlation matrix between the received data of the two orthogonal ULAs can eliminate additive noises, several methods have been proposed by utilizing the cross-correlation matrix [3,7–9]. However, they cannot be extended for the common SRAs. Another drawback of these methods is that they cannot deal with the angle ambiguity problem when multiple sources have the same azimuth or elevation angles. The subspace-based method 2-D MUSIC [2] is suitable for any SRAs and is immune to the angle ambiguity problem. Nevertheless, the 2-D MUSIC requires a 2-D search over the parameter space, which is computationally expensive. Furthermore, the maximum number of detectable sources of the 2-D MUSIC is limited in SRAs, which should be improved.

This work was supported by the National Natural Science Foundation of China under grant No. 61372122, No. 61471205, No. 61302101, No. 61201270 and No. 61302103; the NUPTSF under Grant No. 213012; the Innovation Program for Postgraduate in Jiangsu Province under grant No. KYLX_0813; the Priority Academic Program Development of Jiangsu Higher Education Institutions.

In this paper, we propose a computationally efficient method for 2-D DOA estimation. We first formulate a convex optimization problem for reconstructing the covariance matrix of the coarray and then develop a closed-form solution for the covariance matrix. Finally, the DOAs are retrieved by using the generalized Vandermonde decomposition theorem [10]. Our method has the following advantages: 1) it can be applied to common rectangular array geometries with high estimation accuracy, e.g., URA, L/T-shaped array and SRA with arbitrary geometry; 2) it is computationally efficient because of the closed-form solution. 3) the azimuth and elevation angles are automatically paired; 4) it is immune to the angle ambiguity effect; 5) it is able to locate more sources than directly using the sample covariance matrix.

2. SIGNAL MODEL

We consider a generalized rectangular array (GRA), whose geometry is illustrated in Fig. 1. The sensors are located on a grid with d being the minimum inter-element spacing. The GRAs considered in this paper include the URA and the SRA. The URA contains $\mathcal{N} = N_x \times N_y$ sensors where N_x and N_y are the number of sensors along x- and y-directions, respectively. The SRA can be a URA with some "missing" sensors and we denote the number of its sensors as $\mathcal{M}$, which is small-

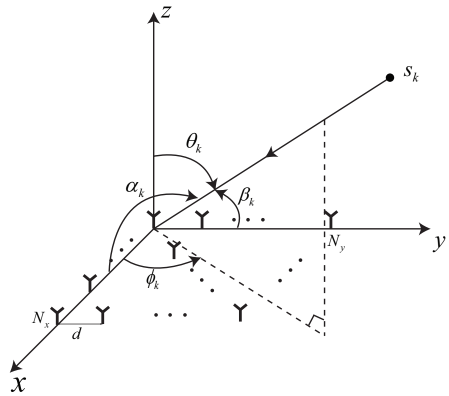

Fig. 1. Array geometry of the GRA.

er than $\mathcal{N}$. In particular, when the SRA is an L-shaped array consisting of two orthogonal ULAs, $\mathcal{M} = N_x + N_y - 1$. For better illustration, we set d to half-wavelength and vectorize the GRA along y-direction. The sensor index set of the new array is defined as $\boldsymbol{\Omega} = \{\Omega_1, \cdots, \Omega_{\mathcal{M}}\}$, where $\boldsymbol{\Omega}$ is sorted in ascending order with $\Omega_1 = 1$. For example, the $\boldsymbol{\Omega}$ with respect to an L-shaped array consisting of two 4-element ULAs equals $\{1, 2, 3, 4, 5, 9, 13\}$. By definition, it is easy to see that $\boldsymbol{\Omega} = \{1, \cdots, \mathcal{N}\}$ in the URA case.

Suppose K far-field narrowband signals impinge onto a GRA as illustrated in Fig. 1 with θ_k and ϕ_k being the elevation and azimuth angles, respectively, and α_k and β_k the electrical angles in x-direction and y-direction of the k-th signal, respectively. From basic geometric knowledge, the electrical angles have the following relations with respect to elevation and azimuth angles,

$$\begin{aligned}\phi_k &= \tan^{-1}\left(\frac{\cos(\beta_k)}{\cos(\alpha_k)}\right)\\ \theta_k &= \sin^{-1}\left(\sqrt{\cos^2(\alpha_k) + \cos^2(\beta_k)}\right).\end{aligned} \tag{1}$$

Hence, when the electrical angles α_k and β_k are retrieved, the physical azimuth and elevation angles can be uniquely determined by (1).

The observation model of the array output with L snapshots is,

$$\boldsymbol{X}_{\boldsymbol{\Omega}} = \boldsymbol{A}_{\boldsymbol{\Omega}}\boldsymbol{S} + \boldsymbol{V}_{\boldsymbol{\Omega}}, \tag{2}$$

where $\boldsymbol{X}_{\boldsymbol{\Omega}} \in \mathbb{C}^{\mathcal{M}\times L}$ is the output of the vectorized version of the GRA along y-direction, $\boldsymbol{A}_{\boldsymbol{\Omega}} = \boldsymbol{\Gamma}_{\boldsymbol{\Omega}}(\boldsymbol{A}_x \odot \boldsymbol{A}_y) = \boldsymbol{\Gamma}_{\boldsymbol{\Omega}}\boldsymbol{A} \in \mathbb{C}^{\mathcal{M}\times K}$ is the manifold matrix of the array, in which $\boldsymbol{\Gamma}_{\boldsymbol{\Omega}} \in \mathbb{C}^{\mathcal{M}\times\mathcal{N}}$ is the selection matrix such that the m-th row of $\boldsymbol{\Gamma}_{\boldsymbol{\Omega}}$ contains all zeros but a single 1 at the Ω_m-th position and $\boldsymbol{A} \triangleq \boldsymbol{A}_x \odot \boldsymbol{A}_y$.[1] $\boldsymbol{A}_x = [\boldsymbol{a}(\alpha_1), \cdots, \boldsymbol{a}(\alpha_K)] \in \mathbb{C}^{N_x\times K}$ and $\boldsymbol{A}_y = [\boldsymbol{a}(\beta_1), \cdots, \boldsymbol{a}(\beta_K)] \in \mathbb{C}^{N_y\times K}$ denote the manifold matrices of the ULAs along x- and y-directions, respectively, where $\boldsymbol{a}_{x_k} = [1, \exp j\pi\sin(\alpha_k), \cdots, \exp j(N_x-1)\pi\sin(\alpha_k)]^T$, $\boldsymbol{a}_{y_k} = [1, \exp j\pi\sin(\beta_k), \cdots, \exp j(N_y-1)\pi\sin(\beta_k)]^T$. With the definitions above, the covariance matrix of $\boldsymbol{X}_{\boldsymbol{\Omega}}$ can be given as,

$$\begin{aligned}\boldsymbol{R}_{\boldsymbol{\Omega}} &= \mathrm{E}[\boldsymbol{X}_{\boldsymbol{\Omega}}\boldsymbol{X}_{\boldsymbol{\Omega}}^H]\\ &= \boldsymbol{\Gamma}_{\boldsymbol{\Omega}}\boldsymbol{A}_{\boldsymbol{\Omega}}\boldsymbol{R}_{\boldsymbol{S}}\boldsymbol{A}_{\boldsymbol{\Omega}}^H\boldsymbol{\Gamma}_{\boldsymbol{\Omega}}^H + \sigma\boldsymbol{I}_{\boldsymbol{\Omega}}\\ &= \boldsymbol{\Gamma}_{\boldsymbol{\Omega}}\mathbb{T}(\boldsymbol{u},\boldsymbol{v})\boldsymbol{\Gamma}_{\boldsymbol{\Omega}}^H + \sigma\boldsymbol{I}_{\boldsymbol{\Omega}}\\ &= \mathbb{T}_{\boldsymbol{\Omega}}(\boldsymbol{u},\boldsymbol{v}) + \sigma\boldsymbol{I}_{\boldsymbol{\Omega}},\end{aligned} \tag{3}$$

where $\mathbb{T}(\boldsymbol{u},\boldsymbol{v}) \in \mathbb{C}^{\mathcal{N}\times\mathcal{N}}$ is a Toeplitz-block-Toeplitz matrix determined only by vectors $\boldsymbol{u} = \left[\boldsymbol{u}^{(1)}; \cdots; \boldsymbol{u}^{(N_x)}\right]$ and $\boldsymbol{v} = \left[\boldsymbol{v}^{(1)}; \cdots; \boldsymbol{v}^{(N_x)}\right]$, σ is the noise power. In particular, $\mathbb{T}(\boldsymbol{u},\boldsymbol{v})$ has the following structure,

$$\mathbb{T} = \begin{bmatrix} T_1 & T_2 & \cdots & T_{N_x}\\ T_{-2} & T_1 & \cdots & T_{N_x-1}\\ \vdots & \vdots & \ddots & \vdots\\ T_{-N_x} & T_{-(N_x-1)} & \cdots & T_1\end{bmatrix}, \tag{4}$$

where T_n is a Toeplitz non-Hermitian matrix with size $N_y \times N_y$, i.e., T_n is determined by $\boldsymbol{u}^{(n)}$ and $\boldsymbol{v}^{(n)}$ where $\boldsymbol{u}^{(n)} \in \mathbb{C}^{N_y}$ equals the first row of T_n and $\boldsymbol{v}^{(n)} \in \mathbb{C}^{N_y-1}$ is the first column of T_n except its first element. Based on the definition, $\mathbb{T}(\boldsymbol{u},\boldsymbol{v})$ can be rewritten as,

$$\mathbb{T}(\boldsymbol{u},\boldsymbol{v}) = \sum_{k=1}^{K} p_k\big(\boldsymbol{a}(\alpha_k)\boldsymbol{a}^H(\alpha_k)\big) \otimes \big(\boldsymbol{a}(\beta_k)\boldsymbol{a}^H(\beta_k)\big), \tag{5}$$

which turns out to be a positive semidefinite matrix with rank K. In practice, the true covariance matrix $\boldsymbol{R}_{\boldsymbol{\Omega}}$ cannot be obtained and is usually estimated with L snapshots as $\hat{\boldsymbol{R}}_{\boldsymbol{\Omega}} = \frac{1}{L}\boldsymbol{X}_{\boldsymbol{\Omega}}\boldsymbol{X}_{\boldsymbol{\Omega}}^H$, where $\hat{\boldsymbol{R}}_{\boldsymbol{\Omega}}$ is error-contaminated due to the finite snapshots. We denote the error component as

$$\begin{aligned}\boldsymbol{E}_{\boldsymbol{\Omega}} &= \hat{\boldsymbol{R}}_{\boldsymbol{\Omega}} - \boldsymbol{R}_{\boldsymbol{\Omega}}\\ &= \hat{\boldsymbol{R}}_{\boldsymbol{\Omega}} - \mathbb{T}_{\boldsymbol{\Omega}}(\boldsymbol{u},\boldsymbol{v}) - \sigma\boldsymbol{I},\end{aligned} \tag{6}$$

where $\boldsymbol{E}_{\boldsymbol{\Omega}}$ consists of signal-signal and signal-noise cross correlation terms which are not $\mathbf{0}$ due to finite snapshot effect. According to [11], the vectorization of $\boldsymbol{E}_{\boldsymbol{\Omega}}$ satisfies the following asymptotic Gaussian distribution,

$$\boldsymbol{W}_{\boldsymbol{\Omega}}^{-\frac{1}{2}}\mathrm{vec}(\boldsymbol{E}_{\boldsymbol{\Omega}}) \sim \mathrm{As}N(\mathbf{0}, \boldsymbol{I}_{\mathcal{M}^2}), \tag{7}$$

where $\boldsymbol{W}_{\boldsymbol{\Omega}} = \frac{1}{L}\boldsymbol{R}_{\boldsymbol{\Omega}}^T \otimes \boldsymbol{R}_{\boldsymbol{\Omega}}$.

3. THE PROPOSED METHOD

According to the extended invariance principle (EXIP) [12], a large-sample maximum likelihood (ML) estimate of $\mathbb{T}(\boldsymbol{u},\boldsymbol{v})$ is obtained by solving the following optimization problem,[2]

$$\min_{\boldsymbol{u},\boldsymbol{v}} \left\|\boldsymbol{Q}\mathrm{vec}(\hat{\boldsymbol{R}}_{\boldsymbol{\Omega}} - \mathbb{T}_{\boldsymbol{\Omega}}(\boldsymbol{u},\boldsymbol{v}) - \sigma\boldsymbol{I})\right\|_2^2, \tag{8}$$

where $\boldsymbol{Q} = \boldsymbol{W}_{\boldsymbol{\Omega}}^{-\frac{1}{2}}$. Problem (8) can be solved by CVX, which however, is time-consuming. In the following, we propose an efficient solution by deriving a closed-form expression. Using the KKT conditions, the optimal solution of (8)

[1] $\boldsymbol{A} \odot \boldsymbol{B}$ denotes the Khatri-Rao product of matrices A and B.

[2] For simplicity, the noise power σ is estimated as the smallest eigenvalue of $\hat{\boldsymbol{R}}_{\boldsymbol{\Omega}}$.

satisfies the following equality,

$$\mathbb{T}^*(\boldsymbol{C}) = \mathbb{T}^*(\boldsymbol{C}\mathbb{T}(\boldsymbol{u},\boldsymbol{v})\boldsymbol{C}), \tag{9}$$

where $\boldsymbol{C} = \boldsymbol{\Gamma}_{\boldsymbol{\Omega}}^T \hat{\boldsymbol{R}}_{\boldsymbol{\Omega}}^{-1} \boldsymbol{\Gamma}_{\boldsymbol{\Omega}}$ and $\mathbb{T}^*(\boldsymbol{C})$ is defined as follows. Let $\boldsymbol{C}$ have the following structure:

$$\boldsymbol{C} = \begin{bmatrix} \boldsymbol{C}_{11} & \boldsymbol{C}_{12} & \cdots & \boldsymbol{C}_{1N_x} \\ \boldsymbol{C}_{21} & \boldsymbol{C}_{22} & & \boldsymbol{C}_{2N_x} \\ \vdots & \vdots & \ddots & \vdots \\ \boldsymbol{C}_{N_x 1} & \cdots & & \boldsymbol{C}_{N_x N_x} \end{bmatrix}, \tag{10}$$

where $\boldsymbol{C}_{mn} \in \mathbb{C}^{N_y \times N_y}$, and let $\boldsymbol{D} = [\boldsymbol{D}_{\mathcal{N}-1}; \cdots; \boldsymbol{D}_{-(\mathcal{N}-1)}]$, where $\boldsymbol{D}_n$ is to take the sum of the n-th diagonal of $\boldsymbol{C}$ in a subarraywise manner. Then $\mathbb{T}^*(\boldsymbol{C})$ is given by $\mathbb{T}^*(\boldsymbol{C}) = T^*(\boldsymbol{D})$, where $T^*(\boldsymbol{\Lambda}) = [w_{-(N-1)}, \cdots, w_{N-1}]^T$, with w_i being the sum of the i-th diagonal of $\boldsymbol{\Lambda}$. Equation (9) can be used to derive a closed-form solution as detailed below.

We first rewrite the right-hand side of (9) as,[3]

$$\mathbb{T}^*(\boldsymbol{C}\mathbb{T}(\boldsymbol{u},\boldsymbol{v})\boldsymbol{C}) = \begin{bmatrix} \boldsymbol{Z}^{(1)} \\ \boldsymbol{Z}^{(2)} \\ \vdots \\ \boldsymbol{Z}^{(N_x)} \end{bmatrix} \begin{bmatrix} \boldsymbol{J}^{(N_x)} \\ \vdots \\ \boldsymbol{J}^{(2)} \\ \bar{\boldsymbol{J}} \end{bmatrix}, \tag{11}$$

where

$$\boldsymbol{Z}^{(n)} = \begin{bmatrix} \mathbb{T}^{*T}\left[\boldsymbol{C}_{:,\boldsymbol{\phi}_1} \boldsymbol{C}_{\{N+1-\boldsymbol{\phi}_1\},:}\right] \\ \vdots \\ \mathbb{T}^{*T}\left[\boldsymbol{C}_{:,\boldsymbol{\phi}_{N_y}} \boldsymbol{C}_{\{N+1-\boldsymbol{\phi}_{N_y}\},:}\right] \\ \mathbb{T}^{*T}\left[\boldsymbol{C}_{:,\boldsymbol{\psi}_1} \boldsymbol{C}_{\{N+1-\boldsymbol{\psi}_1\},:}\right] \\ \vdots \\ \mathbb{T}^{*T}\left[\boldsymbol{C}_{:,\boldsymbol{\psi}_{N_y-1}} \boldsymbol{C}_{\{N+1-\boldsymbol{\psi}_{N_y-1}\},:}\right] \end{bmatrix}, \tag{12}$$

$$\boldsymbol{J} = \begin{bmatrix} \boldsymbol{J}^{(1)} \\ \boldsymbol{J}^{(2)} \\ \vdots \\ \boldsymbol{J}^{(N_x)} \end{bmatrix}, \tag{13}$$

in which,

$$\boldsymbol{\phi}_c = \bigcup_{m=1}^{N_x-n+1} \left\{(m-1)N_y + 1, \cdots, mN_y + 1 - c\right\} \qquad c = 1, \cdots, N_y, \tag{14}$$

$$\boldsymbol{\psi}_d = \bigcup_{m=1}^{N_x-n} \left\{(m-1)N_y + 3 - d, \cdots, mN_y\right\} \qquad d = 1, \cdots, N_y - 1, \tag{15}$$

$$\boldsymbol{J}^{(n)} = \left[u_1^{(n)}, \cdots, u_{N_y}^{(n)}, v_1^{(n)}, \cdots, v_{N_y-1}^{(n)}\right]^T. \tag{16}$$

By using (9), (11) and matrix transformations, we can have,

$$\mathbb{T}^*(\boldsymbol{C}) = [\boldsymbol{Z}_1, \boldsymbol{Z}_2] \begin{bmatrix} \boldsymbol{J} \\ \bar{\boldsymbol{J}} \end{bmatrix} = \boldsymbol{Z}_1 \boldsymbol{J} + \boldsymbol{Z}_2 \bar{\boldsymbol{J}}. \tag{17}$$

[3] $\bar{\boldsymbol{J}}$ denotes the conjugate of $\boldsymbol{J}$. $\boldsymbol{C}_{\mathcal{A},:}$ and $\boldsymbol{C}_{:,\mathcal{B}}$ denote the columns and rows of matrix $\boldsymbol{C}$ indexed by sets $\mathcal{A}$ and $\mathcal{B}$, respectively.

Denoting $\boldsymbol{Y} = \mathbb{T}^*(\boldsymbol{C})$, we finally can have,

$$\underbrace{\begin{bmatrix} \mathcal{R}(\boldsymbol{Y}) \\ \mathcal{I}(\boldsymbol{Y}) \end{bmatrix}}_{\boldsymbol{Y}_r} = \underbrace{\begin{bmatrix} \mathcal{R}(\boldsymbol{Z}_1 + \boldsymbol{Z}_2) & \mathcal{I}(\boldsymbol{Z}_2 - \boldsymbol{Z}_1) \\ \mathcal{I}(\boldsymbol{Z}_1 + \boldsymbol{Z}_2) & \mathcal{R}(\boldsymbol{Z}_1 - \boldsymbol{Z}_2) \end{bmatrix}}_{\boldsymbol{Z}_r} \underbrace{\begin{bmatrix} \mathcal{R}(\boldsymbol{J}) \\ \mathcal{I}(\boldsymbol{J}) \end{bmatrix}}_{\boldsymbol{J}_r}, \tag{18}$$

where $\mathcal{R}(\bullet)$ and $\mathcal{I}(\bullet)$ stand for the real and the imaginary parts of a complex variable, respectively. It is seen from (18) that $\boldsymbol{J}$ can be easily obtained from $\boldsymbol{J}_r = \boldsymbol{Z}_r^{\dagger} \boldsymbol{Y}_r$ where $\dagger$ is the pseudo-inverse operator, i.e., $\mathbb{T}(\hat{\boldsymbol{u}}, \hat{\boldsymbol{v}})$ is also estimated. This closed-form solution has the same precision as using CVX to solve (8) but enjoys a much smaller computational cost.

When the estimate $\mathbb{T}(\hat{\boldsymbol{u}}, \hat{\boldsymbol{v}})$ is determined, the DOAs can be retrieved by the generalized Vandermonde decomposition theorem, recently proposed by Yang [10]. In particular, based on the theorem, $\mathbb{T}(\hat{\boldsymbol{u}}, \hat{\boldsymbol{v}})$ can be decomposed as equation (5), i.e., the DOAs and signal powers are determined simultaneously.

The problem of source enumeration is also an interesting topic and often a prerequisite for DOA estimation. Existing methods such as Akaikes information criterion (AIC), minimum description length (MDL) [13], and second order statistic of eigenvalues (SORTE) [14] are developed based on the covariance matrix. These methods perform well in the URA case but may fail in the SRA case. The reason for this is that the signal subspace expands into the noise subspace in this case. Our method is essentially proposed to reconstruct the covariance matrix of the coarray of the original array. Hence, by simply replacing the sample covariance matrix employed in AIC, MDL and SORTE with $\mathbb{T}(\hat{\boldsymbol{u}}, \hat{\boldsymbol{v}})$, their maximum number of detectable signals can be enlarged. In other words, our method is able to increase the effective aperture size in the case of SRA. In addition, the success rate of source number detection can also be improved compared to most of the original detection methods, which will be investigated in simulations.

4. NUMERICAL RESULTS

In this section, we evaluate the performance of our method via numerical simulations with comparison to 2-D ESPRIT and 2-D MUSIC.[4] In our simulations, we consider two array geometries: a 4×4-element URA and an L-shaped array consisting of two orthogonal 4-element ULAs.

We assume four signals impinge onto the URA from $\boldsymbol{\alpha} = [\alpha_1, \alpha_2, \alpha_3, \alpha_4] = [-15°, -25°, -20°, 0°]$ and $\boldsymbol{\beta} = [\beta_1, \beta_2, \beta_3, \beta_4] = [10°, 0°, 30°, 5°]$. The SNR is fixed at 0dB and 100 snapshots are collected. We compare the DOA estimates of our method and 2-D ESPRIT based on 500 independent trials in Fig. 2. Black circles denote the true DOAs and different colored dots denote the estimated ones with respect to different DOAs. We can conclude from the scattergram in Fig. 2(a) that these four DOAs are clearly detected, while 2-D ESPRIT almost fails to separate these signals. In particular, our method outperforms 2-D ESPRIT in view of

[4] Since 2-D MUSIC requires 2-D searching which is time-consuming for simulation, we only consider 2-D ESPRIT in estimation performance comparison. When the detection performance is evaluated, we only employ the 2-D MUSIC for comparison since 2-D ESPRIT is unapplicable for the SRA.

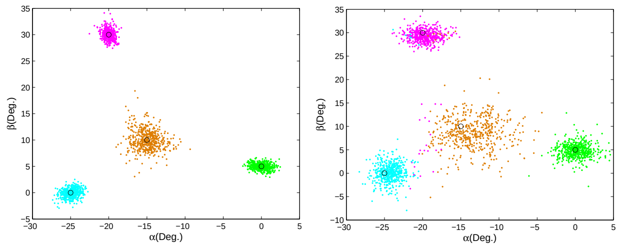

(a) Proposed (b) 2-D ESPRIT

Fig. 2. 2-D DOA estimates scattergrams of our method and 2-D ESPRIT.

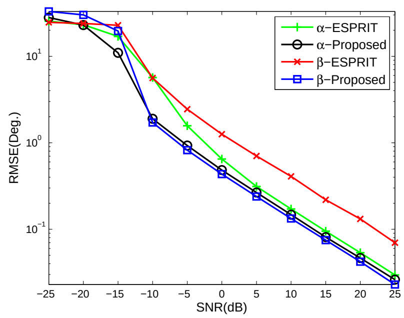

Fig. 3. Performance comparison of our method and 2-D ESPRIT.

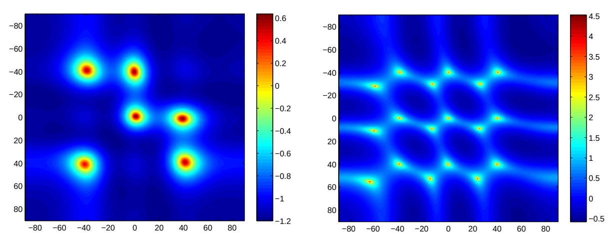

(a) Proposed (b) 2-D MUSIC

Fig. 4. 2-D DOA estimates contour of our method and 2-D MUSIC.

two observations. First, the boundary of the scattergram in Fig. 2(a) is clearer than that in Fig. 2(b). Second, there exists a leakage between the scattergrams of the DOAs in Fig. 2(b), which is not observed in Fig. 2(a).

Next, we compare the estimation performance of the proposed method and 2-D ESPRIT with respect to different SNRs. We assume four signals impinge onto the URA from $\boldsymbol{\alpha} = [10°, -20°, 30°, 0°]$ and $\boldsymbol{\beta} = [-50°, -30°, -20°, 0°]$. The RMSEs of our method and 2-D ESPRIT with respect to $\boldsymbol{\alpha}$ and $\boldsymbol{\beta}$ are compared in Fig. 3 with SNR varying from -25dB to 25dB. The number of collected snapshots is set to 100. We can see that the RMSEs of our method with respect to both $\boldsymbol{\alpha}$ and $\boldsymbol{\beta}$ are lower than that of 2-D ESPRIT in most cases of the compared SNR range. In particular, when SNR≥ -10dB, although the difference between 2-D ESPRIT and the proposed method with respect to $\boldsymbol{\alpha}$ becomes smaller, the gap between the two methods with respect to $\boldsymbol{\beta}$ is still large.

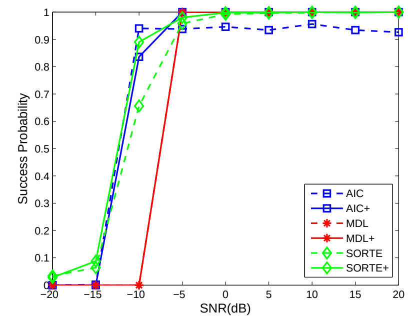

Fig. 5. Detection performance comparison of AIC(+), MDL(+) and SORTE(+).

Then, we compare the detection performance of our method and 2-D MUSIC with the L-shaped array. Assume six independent narrowband signals impinge onto the array from $\boldsymbol{\alpha} = [-40°, 0°, 0°, -40°, 40°, 40°]$ and $\boldsymbol{\beta} = [0°, 40°, 0°, -40°, -40°, 40°]$. We employ 400 snapshots and set SNR$=$ 10dB. We plot the contours of the 2-D DOA estimates of our method and 2-D MUSIC in Fig. 4, from which it is obvious that our method is able to locate all the six signals correctly while 2-D MUSIC fails. Note that, although several sources have the same azimuth or elevation angles, our method is immune to the angle ambiguity effect.

Finally, we carry out simulation to show the detection performance of our DOA estimator. The original AIC, MDL and SORTE methods employ $\hat{\boldsymbol{R}}_{\boldsymbol{\Omega}}$ when detecting the source number while our modified ones employ $T(\hat{\boldsymbol{u}})$ and the corresponding methods are denoted as AIC+, MDL+ and SORTE+, respectively. Fig. 5 shows the detection performance of AIC+, MDL+ and SORTE+ with SNR varying from -20dB to 20dB. We can see that SORTE has a better detection performance when our method is employed; the performance of AIC+ increases more than 10% percent compared to AIC when SNR≥ -5dB; the performance of MDL+ is comparable to that of MDL. Overall, our method enhances the performance of the source enumeration methods with only a little computational cost added.

5. CONCLUSION

A computationally efficient method for 2-D DOA estimation has been proposed in this paper. Our method can be applied to the SRAs with arbitrary geometries and is of high estimation accuracy. The azimuth and elevation angles have been paired automatically. Moreover, the proposed method is immune to the angle ambiguity effect and able to locate more sources than conventional subspace-based methods.

6. REFERENCES

[1] P. Heidenreich, A. M. Zoubir, and M. Rubsamen, "Joint 2-d doa estimation and phase calibration for uniform rectangular arrays," *IEEE Transactions on Signal Processing*, vol. 60, no. 9, pp. 4683–4693, Sept 2012.

[2] M. G. Porozantzidou and M. T. Chryssomallis, "Azimuth and elevation angles estimation using 2-d music algorithm with an l-shape antenna," in *2010 IEEE Antennas and Propagation Society International Symposium*, July 2010, pp. 1–4.

[3] J. F. Gu and P. Wei, "Joint svd of two cross-correlation matrices to achieve automatic pairing in 2-d angle estimation problems," *IEEE Antennas and Wireless Propagation Letters*, vol. 6, pp. 553–556, 2007.

[4] M. D. Zoltowski, M. Haardt, and C. P. Mathews, "Closed-form 2-d angle estimation with rectangular arrays in element space or beamspace via unitary esprit," *IEEE Transactions on Signal Processing*, vol. 44, no. 2, pp. 316–328, Feb 1996.

[5] Matteo Carlin, Paolo Rocca, Giacomo Oliveri, and Andrea Massa, "Bayesian compressive sensing as applied to directions-of-arrival estimation in planar arrays," *Journal of Electrical & Computer Engineering*, vol. 2013, no. 12, 2013.

[6] Y. Hua, T. K. Sarkar, and D. D. Weiner, "An l-shaped array for estimating 2-d directions of wave arrival," *IEEE Transactions on Antennas and Propagation*, vol. 39, no. 2, pp. 143–146, Feb 1991.

[7] G. Wang, J. Xin, N. Zheng, and A. Sano, "Computationally efficient subspace-based method for two-dimensional direction estimation with l-shaped array," *IEEE Transactions on Signal Processing*, vol. 59, no. 7, pp. 3197–3212, July 2011.

[8] N. Tayem and H. M. Kwon, "L-shape 2-dimensional arrival angle estimation with propagator method," in *2005 IEEE 61st Vehicular Technology Conference*, May 2005, vol. 1, pp. 6–10 Vol. 1.

[9] J. F. Gu, W. P. Zhu, and M. N. S. Swamy, "Joint 2-d doa estimation via sparse l-shaped array," *IEEE Transactions on Signal Processing*, vol. 63, no. 5, pp. 1171–1182, March 2015.

[10] Z. Yang, L. Xie, and P. Stoica, "Vandermonde decomposition of multilevel toeplitz matrices with application to multidimensional super-resolution," *IEEE Transactions on Information Theory*, vol. PP, no. 99, pp. 1–1, 2016.

[11] Zhang-Meng Liu, Zhi-Tao Huang, and Yi-Yu Zhou, "Sparsity-inducing direction finding for narrowband and wideband signals based on array covariance vectors," *IEEE Transactions on Wireless Communications*, vol. 12, no. 8, pp. 1–12, August 2013.

[12] Björn Ottersten, Peter Stoica, and Richard Roy, "Covariance matching estimation techniques for array signal processing applications," *Digital Signal Processing*, vol. 8, no. 3, pp. 185–210, 1998.

[13] M. Wax and T. Kailath, "Detection of signals by information theoretic criteria," *IEEE Transactions on Acoustics, Speech and Signal Processing*, vol. 33, no. 2, pp. 387–392, Apr 1985.

[14] Zhaoshui He, A. Cichocki, Shengli Xie, and Kyuwan Choi, "Detecting the number of clusters in n-way probabilistic clustering," *IEEE Transactions on Pattern Analysis and Machine Intelligence*, vol. 32, no. 11, pp. 2006–2021, Nov 2010.